Material Design Using Molecular Modeling for Hydrogen Storage

F. Darkrim Lamari, B. Weinberger, and M. Kunowsky
LIMHP Université Paris 13, CNRS UPR 1311, 93430 Villetaneuse, France

D. Levesque
LPT UMR CNRS 8627, Université Paris XI, Bâtiment 210, 91405 Orsay, France

DOI 10.1002/aic.11670
Published online January 2, 2009 in Wiley InterScience (www.interscience.wiley.com).

Using grand canonical Monte-Carlo simulations, the adsorption capacities and isosteric heats of hydrogen on activated carbons, graphite nanofibers, and bundles of carbon nanotubes are estimated for identical thermodynamic states. These computations allow a systematic, meaningful, and unbiased comparison of the adsorption properties of hydrogen in such porous materials. The comparison shows that the hydrogen storage capacity can be optimized, but only to a limited extent, in adjusting the material pore sizes and functionalizing a part of the adsorption sites. Therefore, at room temperature and up to 70.0 MPa, for the three models of carbonaceous adsorbents, the hydrogen maximal excess adsorption is of the order of 2% of the adsorbent mass.
 AIChE J, 55: 538–547, 2009
Keywords: adsorption/gas, computer simulation (MC and MD), porous media

Introduction

For the practical applications such as the purification or storage, the relevant physical property of porous materials is their capacity to adsorb the gases or fluids.[1] This capacity is characterized by the amount m_a of adsorbed gases per gram of adsorbent material. m_a is measured at a macroscopic scale, but its value results from adsorption processes which, at the microscopic scale, differ significantly with the size and shape of the pores. In pores, larger than few nanometers, the central part of the pores can be filled by a gas with a density and temperature identical to those of the bulk gas surrounding the porous material. Clearly, the partial filling of the pore network by the bulk phase is not characteristic of the adsorbent properties because it is similar to the gas expansion in an empty volume. This remark leads to define the excess adsorption m_e which, for the adsorption of a pure gas, is given by $m_e = m_a - \rho_b V_f$. ρ_b is the density of the gas in the bulk phase per volume unit and V_f the free volume or volume accessible to gas in the porous material per gram of adsorbent.[2]

In this work, for hydrogen at room temperature (293 K), the values of m_a, m_e, and isosteric adsorption heats q_i are computed for pore models of activated carbons, adsorbents formed with single-walled (SW) carbon nanotubes, or graphite nanofibers (GNF). In spite of the complexity of pore networks at the macroscopic or mesoscopic scales, these models are expected to describe the types of pores present in the materials contributing mainly to the adsorption processes.

Similar models, in particular of activated carbons and adsorbents of SW nanotubes, have been already studied in the literature by numerical simulations.[3–17] In these models, the potentials describing the interactions between hydrogen molecules and between these molecules and the adsorbent, although they are qualitatively similar (van der Waals interaction), differ quantitatively. The hydrogen–hydrogen interaction is described by Lennard–Jones (LJ) pair potentials (cf. definition later) in the works,[3–5,8,10,11,14–17] but with various parametrizations, or by a Silvera–Goldman pair potential[18] in the works.[6,7,12,13] In addition, the electric quadrupole of hydrogen molecules is taken into account in the articles.[8,11]

Correspondence concerning this article should be addressed to F. D. Lamari at fdl@limhp.univ-paris13.fr.

For the hydrogen-material interactions, also of the van der Waals type, the articles[5,10,15,17] use the Steele interaction,[19] an interaction averaged on the pair potentials between hydrogen and carbon atoms inside the pore walls, the articles[6,7] use a different, but similar, interaction, the Crowell–Brown interaction[20] or a modified Crowell–Brown interaction.[7] In the articles,[3,5,8,14,16] all pair interactions between hydrogen molecule and carbon atom, which are described by a LJ potential, are independently summed. Quantum effects are considered in the articles.[6,8] The simulations, realized near the room temperature, were performed at temperatures of 175,[16] 293,[3,5,11,14] 298,[6,7,10,12,13,15,17] or 300 K[4] and pressures below 20.0 MPa.

The set of simulation results, presented in this article, is free of systematic differences between molecular interactions or considered thermodynamic states. It allows to appreciate without any bias the variations between the hydrogen adsorption and storage efficiencies and isosteric heat values of the considered adsorbent models, because the specific surfaces (adsorbent surface per gram of material) and free volumes, used to compute m_e, are estimated by identical and coherent procedures (cf. later).

First, we describe the pore models studied in the simulations and give the essential informations on the Grand Canonical Monte-Carlo (GCMC) method used for computing the adsorption properties.[21,22] Next, the results obtained for the different pore models of activated carbons, SW carbon nanotubes, and GNF are presented. Then, the analysis and discussion of the simulation results lead to remarks on the optimization of the storage capacity of carbonaceous adsorbents at room temperature and pressures up to 70.0 MPa.

Description of Adsorbent Models

In the activated carbons, the main type of pores are expected to be slits with various widths, which have walls formed by one graphite basal plane or stacks of 2, 3, or more planes, parallel to the slit.[23] In this study, we estimate the H_2 adsorption in such slit pores with walls made up of 1, 2, or 3 graphite basal planes, denoted AC1, AC2, and AC3, we consider two values of the slit width d_s: 1.0 and 2.5 nm. AC1, AC2, and AC3 correspond to porous materials with specific surfaces equal to $\sim$2600, 1300, and 900 m^2/g, respectively.[24,25] The widths correspond to two specific cases of adsorption: the case where, because of the size of H_2 molecules, at the most, two layers of molecules located near the walls can be adsorbed inside the pore (width of 1.0 nm), and that where these layers are in equilibrium with a bulk phase filling the central part of the pore (width of 2.5 nm).

At the microscopic scale, the adsorbent made up of SW carbon nanotubes[26] is composed of parallel nanotubes arranged on a triangular lattice in a plane perpendicular to the tube axes. In such arrangements, the nanotubes form bundles. The adsorption capacity of these bundles varies between the case where the nanotubes are closed and close-packed, and that where the nanotubes are opened and located on an expanded triangular lattices.[27] For the bundle of 30 close-packed closed SW nanotubes, considered in our simulations, the contribution of the external surface to the specific surface is of the order of $\sim$240 m^2/g and that of the narrow interstitial domains located between the nanotubes of the order of $\sim$200 m^2/g. When in the close-packed bundle, the nanotubes are opened, the tube internal surface becomes accessible and the specific surface is $\sim$1500 m^2/g. For the expanded bundle of opened nanotubes, the specific surface is $\sim$2600 m^2/g. Between the extreme values, all intermediate values of the specific surface are possible, in particular when the nanotubes are partially opened.

We consider GNF materials where, at the microscopic scale, the pores are slits with walls composed of stacks of graphite basal planes.[28,29] The planes are perpendicular (GNF1 model) or tilted (GNF2 model) with respect to the stacking direction.[30] With this pore configuration, the GNF adsorbent surface is constituted by the zigzag edges of graphite basal planes and, so, carbon atoms which, having a pending chemical bond, are functionalized.[31] The properties of these adsorbent surfaces depend on the type of functional groups. In our simulations, we consider the groups H and CH_3. The two stacks, limiting the slits, are separated by d_s, the distance between the external functionalized carbon atoms. For similar reasons to those mentioned for the models of activated carbons, we consider values of d_s ranging from 0.7 to 3.0 nm. The value of the GNF specific surface is strongly dependent on the transverse size D of the fiber, i.e., the thickness of the stack between the slits located at its boundaries. In our simulations, D is equal to 1.0 nm, i.e., the extension of about three hexagons of carbon atoms in a graphite basal plane. With this D value, the specific surface is $\sim$1030 m^2/g, similar to that of the AC3 model. Clearly, larger D values would lead to smaller specific surfaces.

In the literature,[32,33] it is mentioned that the GNF structure could be modified by increasing the spacing d_p between the graphite planes of the stacks. The consequence of such a change has been studied by considering the adsorption capacities of the GNF2 model when the graphite basal planes are spaced at distances d_p equal to 0.68 and 0.9 nm. Such arrangements, which, possibly, could be obtained by an intercalation process, correspond to models of carbonaceous porous materials where important parts ($\sim$20%) of adsorption sites are functional groups. When d_p becomes equal to or larger than 0.68 nm, H_2 molecules can be adsorbed inside the stack of graphite basal planes, the specific surface increases and can reach a value of $\sim$2600 m^2/g, similar to that of the AC1 model.

The value of the free volume V_f, needed for computing the excess adsorption, can be obtained experimentally by the helium displacement method.[34] To be in agreement with this procedure, the helium adsorption has been computed by simulation at 653 K and a pressure of 0.1 MPa. From the amount of helium adsorbed in the pore models and by supposing that, as it is done in the experimental procedure, the excess adsorption of helium is zero, it is easy to determine V_f from the relation $V_f = m_a^{He}/\rho_b^{He}$ where ρ_b^{He} is the helium bulk density at 0.1 MPa and 653 K and m_a^{He} is the mass of helium adsorbed per gram of adsorbent. The solid skeleton density is given by $\rho_s = 1.0/(V_t - V_f)$ where V_t is the total volume occupied by 1 g of adsorbent. In the simulations,[3–17] m_e is not estimated or estimated by different methods. An effective slit size[10] can be used for the calculation of V_f as it was proposed by Kaneko et al.[35] m_e can be also defined as the difference between the amount of H_2 present in the simulation box with the adsorbent and the amount of H_2 present in this box without the adsorbent.[3,4,7]

Table 1. Parameters ε and σ of the LJ potentials for H_2 Molecules, C Atoms in Activated Carbons, Nanotubes, or GNF, and CH or CH_3 Chemical Groups in GNF

	ε (K)	σ (Å)	q_e (e)	l (Å)
H_2	36.7	2.958	0.483	0.3705
C	28.0	3.400	–	–
CH	46.0	3.770	–	–
CH_3	100.0	3.850	–	–

l distance to the center of mass along the symmetry molecular axis of the effective charges q_e (unit of electron charge: e) associated to the H_2 quadrupole.

For the activated carbon models, ρ_s is equal to 2.18 (AC1), 2.25 (AC2), and 2.26 g/cm^3 (AC3), close to the value obtained for a perfect crystal of graphite: 2.26 g/cm^3. For the GNF models, the ρ_s values are similar: 1.9 (compact GNF1 and GNF2 models) or 2.1 g/cm^3 (expanded GNF2 model). In the case of nanotube bundles, ρ_s has a value depending on the possibility that helium can to be adsorbed inside the nanotubes. A value of $\sim$1.8 g/cm^3 is obtained for an expanded bundle of 30 opened nanotubes and $\sim$1.3 g/cm^3 for a close-packed bundle of 30 closed nanotubes.

The previous description of the pore models is completed by the specification of the interactions between H_2 molecules and adsorbents given in Table 1. The interactions are pair potentials of LJ type with the generic expression: $v_{LJ}(r_{ij}^{\alpha\beta}) = 4\varepsilon_{\alpha\beta}\left[\left(\sigma^{\alpha\beta}/r_{ij}^{\alpha\beta}\right)^{12} - \left(\sigma^{\alpha\beta}/r_{ij}^{\alpha\beta}\right)^{6}\right]$ where $r_{ij}^{\alpha\beta}$ is the distance between the atoms or molecular centers of mass i and j of species α and β in the adsorbed gas or solid adsorbent. The LJ parameters of the cross-interactions are obtained from Table 1 by using the Berthelot's rule, expressed by the relations: $\sigma^{\alpha\beta} = 0.5\ (\sigma^{\alpha\alpha} + \sigma^{\beta\beta})$ and $\varepsilon^{\alpha\beta} = (\varepsilon^{\alpha\alpha}\ \varepsilon^{\beta\beta})^{1/2}$. In the simulations, the LJ potentials are truncated at a distance of $\sim$1.6 nm, i.e., a distance where they are equal to $\sim 5 \times 10^{-5}$ times the minimal value of the LJ potential. In addition, the H_2 molecule has a linear quadrupole, which is described by three effective charges: two located at the proton positions of values q_e and one at the center of mass with a value $-2q_e$.[36]* For the activated carbon models, the energy minimum and interaction range are in close agreement with theoretical estimates based on density functional theory.[37]

In the GNF models, the functional groups are described by using the united atoms approximations.[38,39] The LJ potentials of CH groups are centered on the carbon atoms at the graphite plane ends. The LJ potentials of the CH_3 groups are centered at a distance equal to 0.142 nm of these latter carbon atoms. For identical d_s, the free volume of the GNF functionalized by CH_3 groups is smaller than that of the GNF functionalized by CH groups because of the excluded volume effects of the CH_3 groups.

The total and excess adsorptions have been computed by using the GCMC method, an algorithm peculiarly adapted to the simulation of adsorption processes.[21,22] The MC runs comprise an equilibrium phase of 2.0–4.0 $\times$ 10^6 MC trial moves (displacement, deletion, or insertion of gas molecules) followed by 12.0–16.0 $\times$ 10^6 MC moves, which allow a computation of the average values of m_a and q_i.[21,40] These quantities are given by:

$$m_a = \frac{\langle N\rangle M_H}{N_C M_C + N_H M_H} \quad (1)$$

$$q_i = H_b - \frac{\langle NU\rangle - \langle N\rangle\langle U\rangle}{\langle N^2\rangle - \langle N\rangle^2}. \quad (2)$$

$\langle..\rangle$ denotes a GC average and H_b is the enthalpy of the bulk gas, easily computed by MC simulations. $\langle U\rangle$ and $\langle N\rangle$ are, respectively, the average of the total energy U and number N of adsorbed gas molecules. M_C and M_H being the molar masses of C and H, N_C and N_H the numbers of carbon and hydrogen atoms, chemically bonded to carbon atoms in the adsorbent models, m_a is given in g/g. The statistical error on the m_a values is estimated to be of the order of 1–2% that on q_i is larger and equal to 3–5% because its value is obtained from a fluctuation ratio. The isosteric heat is an important physical characteristic of an adsorption process, in particular for a storage application when the entire adsorption–desorption cycle is considered.[41] The optimum values of the adsorption enthalpy change for hydrogen adsorption processes are discussed, for instance, by Gigras et al.[17] and Bhatia and Myers.[42]

For all systems, the simulation volumes are parallelepipedic cells with periodic boundary conditions. The coordinate axes being parallel to the cell walls, for the AC1, AC2, and AC3 models, the slits are parallel to the xoy plane and the pore walls replicated in the x and y directions, while the patterns constituted by the planes and slits are replicated in the z direction. In the simulation cell of the AC1 model, there are six slits with walls made up of one graphite basal plane. In the cell of the AC2 model, there are three slits with walls made up of two graphite basal planes, and in the cell of the AC3 model, two slits with walls made up of three graphite basal planes. Each graphite basal plane contains 1320 carbon atoms. For the AC1, AC2, and AC3 models, the sizes of the cells are equal to 27.44 σH_2H_2 and 14.40 σH_2H_2 in the x and y directions, respectively. In the z direction, for the AC1 model, the size is equal to 20.28 σH_2H_2 (d_s = 1.0 nm) or 50.71 σH_2H_2 (d_s = 2.5 nm). For the AC2 and AC3 models, it is, respectively, equal to 13.53 σH_2H_2 (d_s = 1.0 nm) or 28.75 σH_2H_2 (d_s = 2.5 nm) and 11.29 σH_2H_2 (d_s = 1.0 nm) or 21.43 σH_2H_2 (d_s = 2.5 nm).

The bundles of 30 nanotubes are parallel to the y axis and the tubes are periodically replicated in the y direction. The simulation cell has the following sizes: 50.88 σH_2H_2 in the x direction, 11.52 σH_2H_2 in the y direction, and 52.22 σH_2H_2 in the z direction. It contains 16,320 carbon atoms (544 per nanotube).

For the GNF models, the simulation cell contains two stacks of 16 graphite planes. Each stack is formed by 2720 carbons atoms, comprising the 544 carbon atoms of the CH_3 functional groups, or by 2176 carbons atoms, comprising the 544 carbon atoms of the CH functional groups. The stacks are parallel to the xoz plane, replicated in the x and z directions and the pattern constituted by the stacks and slits is replicated in the y direction. The stacks form two slit pores

*At 293 K, the validity of the hydrogen–hydrogen interaction given in Table 1 is established by comparison between data from the NIST chemistry webbook (http://webbook.nist.gov) and GCMC simulation results obtained for the bulk phase. At 0.51 MPa the hydrogen density is 0.2087 (NIST data) and 0.2087 mol/l (GCMC results), at 1.0, 10.0, 30.0, and 70.3 MPa the densities are 0.4080 and 0.4082, 3.867 and 3.880, 10.35 and 10.43, and 19.79 and 20.0, respectively.

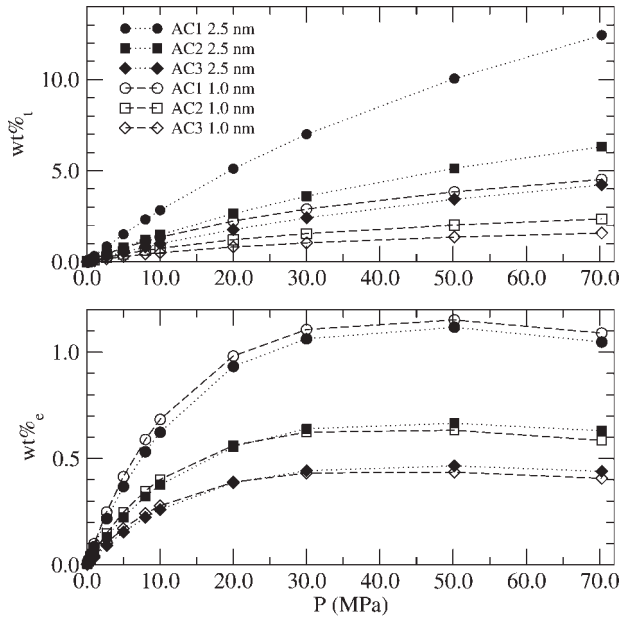

Figure 1. Total (wt $\%_t$) and excess (wt $\%_e$) adsorptions for activated carbon models AC1, AC2, and AC3 with slit widths equal to 1.0 nm and 2.5 nm at $T = 293$ K.

in taking into account the periodical boundary conditions. The cell sizes are equal to 14.13 σH_2H_2 and 18.11 σH_2H_2 in the x and z directions. In the y direction, the size varies between 10.49 σH_2H_2 and 26.04 σH_2H_2 when d_s varies between 0.7 and 3.0 nm.

To perform a GCMC simulation of an adsorption process, it is needed to know the chemical potential corresponding to the thermodynamic state of the bulk gas in contact with the adsorbent. In this work, this correspondence between chemical potential and pressure was determined by GCMC simulations of H_2 bulk gas. For a given volume, temperature, and chemical potential, the pressure was computed in the GCMC run by the virial theorem. The value of the chemical potential was adjusted until the pressure is the required value for H_2 bulk gas. These simulations also give the bulk enthalpy H_b used in the computation of q_i.

Simulation Results

Activated carbon models

Estimates of m_a and m_e for the AC1, AC2, and AC3 models are presented in Figure 1. For all models, the total adsorptions are expressed in wt $\%_t$ defined as 100 m_a, m_a being the mass of adsorbed gas per gram of adsorbent (cf. Eq. 1). For identical slit width and pressure, the ratios of wt $\%_t$ values between the different models are close to those between their specific surfaces. The data show an important increase of wt $\%_t$ when the slit width grows from 1.0 to 2.5 nm. For this latter width, wt $\%_t$ of the AC1 model reaches $\sim$12% at 70.0 MPa.

However, the plots of m_e, expressed in wt $\%_e$ (i.e., 100 m_e), given in Figure 1, show that the wt $\%_t$ large values correspond, at a large extent, to compression effects. When the contributions of these effects are removed, the excess adsorption isotherms are similar for the models with the same specific surface whatever the slit width. The interpretation of these data arises mainly from the range and strength of the interactions between H_2 and the pore walls. These characteristics are manifested by the local density profiles drawn in Figure 2: the layers of adsorbed molecules are located near the walls and, in the pore domain where the hydrogen-adsorbent interactions are near zero, the pore is filled with the bulk gas. Therefore, for a given thermodynamic state of the H_2 bulk phase, when the pores have a width sufficient for allowing the formation of one layer on each wall, the layer density profiles and m_e values depend weakly on the width size.

Small corrections to these qualitative results come from the excluded volume effects in the adsorbed layers, which become important at high pressures: in narrow pores the density in the central part becomes smaller than the bulk density and, in large pores, the onset of a second adsorbed layer is clearly visible (cf. Figure 2). These corrections do not modify appreciably the typical variation of the excess adsorption isotherms characterized by the saturation of the excess adsorption for pressures larger than 20.0 MPa. Above this pressure, the increase of the total adsorption is balanced almost exactly by that of the bulk gas density.

The value of q_i is computed by noticing that Eq. 2 writes at a given temperature[40]:

$$q_i = H_b - \frac{\langle UN\rangle - \langle U\rangle\langle N\rangle}{\langle N^2\rangle - \langle N\rangle^2} = P\Big/\rho_b + u_b^c + u_b^i - u_a^c - \frac{\langle U_a^i N\rangle\langle U_a^i\rangle\langle N\rangle}{\langle N^2\rangle - \langle N\rangle^2} \tag{3}$$

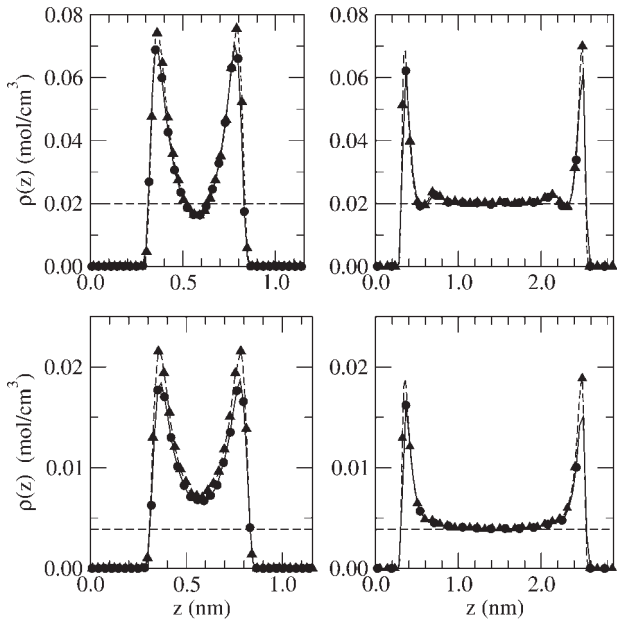

Figure 2. At $T = 293$ K, comparison of density profiles $\rho(z)$ at 10 (bottom row) and 70.0 MPa (top row) for the activated carbon models.

AC1 (solid line and filled circle) and AC3 (dashed line and filled triangle up) with the slit widths: 1.0 nm (left column) and 2.5 nm (right column). Horizontal dashed lines: bulk density values at 10.0 or 70.0 MPa.

where u_b^c and u_a^c are the average kinetic energies per molecule, equal to 5 $k_BT/2$ for H_2 in the bulk and adsorbed phases. u_b^i is the internal energy per molecule of the bulk phase and U_a^i the internal energy of the adsorbed phase. u_b^c being equal to u_a^c at the adsorption equilibrium, Eq. 3 becomes:

$$q_i = k_BT - \frac{\langle U_a^i N\rangle - \langle U_a^i\rangle\langle N\rangle}{\langle N^2\rangle - \langle N\rangle^2}, \quad (4)$$

when $P/\rho_b \sim k_BT$ and $u_b^i \sim 0.0$, i.e., when the bulk phase is supposed to be a perfect gas.

The results of the q_i computation using Eq. 3 are presented in Figure 3. The confinement of the adsorbed gas modifies the q_i values, which are increased by ~30–50% when d_s varies from 2.5 to 1.0 nm. At constant d_s, the q_i variations between the three models result from the increase of H_2-wall interactions and are equal to ~10%. These quantitative differences are closely linked to the density profiles displayed in Figure 2. For instance at d_s = 1.0 nm, these profiles show that, the adsorbed layers being distant by ~0.35 nm, the interaction between molecules located in different layers can significantly contribute to U_a^i. This latter contribution does not exist in the large pore (d_s = 2.5 nm) where the adsorbed layers are in equilibrium with the bulk phase. The peak height of the AC3 density profile is higher than that of the AC1 profile, in agreement with the increase of the H_2-wall interaction for the AC3 model. At the pressures smaller than 5.0 MPa, it is found that Eqs. 3 and 4 give almost identical results within statistical errors.

At similar pressures and temperatures, our results are in agreement with those of previous simulations obtained for models of slit pores, which are expected to have equivalent specific surfaces and free volumes. For instance, at 10.0 MPa and 293 K, the AC1 model with d_s = 1.0 nm gives wt $\%_t$ = 1.34 and wt $\%_e$ = 0.68. This result can be compared with those found at 10.0 MPa and 300 K by Rzepka et al.[4] for a slit with d_s = 1.0 nm: wt $\%_t$ = 1.30, and by Craknell[10] at 10.0 MPa and 298 K, for slits with d_s = 0.9 nm: wt $\%_t$ = 1.2 and wt $\%_e$ = 0.6, and d_s = 1.2 nm wt $\%_t$ = 1.78 and wt $\%_e$ = 0.7.

At 3.0 MPa and 298 K, Gigras et al.[17] give wt $\%_t$ = 0.48, 0.28, and 0.18 for models similar to AC1, AC2, and AC3 with d_s = 1.0 nm; for an identical slit width, we obtain, at 2.72 MPa and 293 K, wt $\%_t$ = 0.44 (AC1), 0.25 (AC2), and 0.17 (AC3). These agreements confirm that there are only small differences in the estimated adsorption capacities of slit pore models when the specific surface and free volume of the models are close and known, and acceptable interactions are used in the simulations.

Single-walled nanotube models

In previous publications, the adsorption on lattices or bundles of (n,0) or (n,n) SW carbon nanotubes at room temperature has been computed.[3,6,8,9,14] In particular, the diameter of (n,0) SW nanotubes leading to a maximal excess adsorption was estimated to be equal to D_n = 1.33 nm ((17,0) SW nanotube). Here, we report the results of simulations performed for bundles of 30 (17,0) SW nanotubes, packed in a triangular arrangement. We consider an adsorbent model,

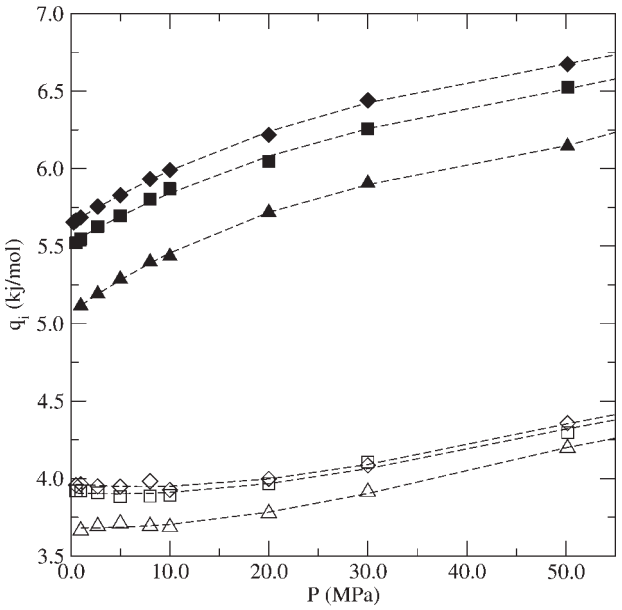

Figure 3. Simulation results for q_i obtained from Eq. 3.

AC1 model, d_s = 1.0 nm: filled triangle up and d_s = 2.5 nm: open triangle up. AC2 model, d_s = 1.0 nm: filled square, and d_s = 2.5 nm: open square. AC3 model, d_s = 1.0 nm: filled diamond, and d_s = 2.5 nm: open diamond.

where the bundles are distant in average by more than ~2.0 nm. Because the interaction range near the external surface of a bundle is ~0.4 nm, the adsorption properties of the model are described by those of a single bundle.

When in the bundle, the SW nanotubes are close-packed, the minimal distance d between the walls of neighboring tubes is 0.34 nm, similar to that found in the experimental samples.[43–45] The adsorption properties of an expanded bundle where d is equal to 0.6 nm is also computed. This latter arrangement, which possibly can be obtained by an intercalation molecular process,[32] is favorable for the adsorption. When the nanotubes are opened, both external and internal surfaces of the walls are accessible to H_2 and, for d = 0.6 nm, the nanotubes stay sufficiently close for minimizing, inside the bundle, the internal volume where the interactions between H_2 and nanotubes are near zero.

In this model, where does not exist a contribution to the adsorption induced by cooperative interactions between bundles, m_a is not significant. m_a results mainly from the compression effects due to the filling by the bulk gas of the void volume between bundles, and we discuss only the results for m_e. Figure 4 displays the wt $\%_e$ values for the four cases of closed or opened nanotubes arranged in a close-packed or expanded bundle. The excess adsorptions isotherms are qualitatively similar for the adsorbent four models. The excess adsorption isotherms of the expanded bundle of opened nanotubes and that of the AC1 model are in good quantitative agreement with a maximal value of wt $\%_e$ ~1.2%, an expected result because both adsorbent models have similar specific surfaces and H_2-adsorbent interactions.

The maximal value of wt $\%_e$ of the close-packed and closed nanotubes is comparable to that of the AC3 model. This agreement at large pressures (~70.0 MPa) does not stay

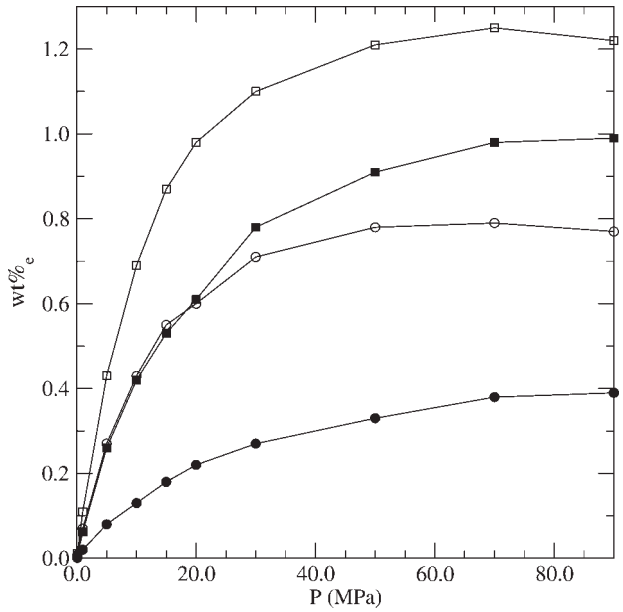

Figure 4. At T = 293 K, excess adsorption isotherms (wt $\%_e$) for bundles of 30 opened or closed SW nanotubes of diameter D_n = 1.33 nm.

Closed nanotubes and packed bundle (d = 0.34 nm): filled circle. Opened nanotubes and packed bundle (d = 0.34 nm): filled square. Closed nanotubes and expanded bundle (d = 0.60 nm): open circle. Opened nanotubes and expanded bundle (d = 0.60 nm): open square.

at lower pressures. The bundle excess adsorption increases toward its maximum more slowly with the pressure. For instance, at 20.0 MPa, wt $\%_e$ is equal to 0.18 for the bundle and 0.39 for the AC3 model. The bundle excess adsorption is larger than expected from the value of its specific surface ($\sim$500 m^2/g) compared with that of the AC3 model ($\sim$900 m^2/g). The low value of the bundle specific surface is compensated by the large minimal potential energies, very favorable for the adsorption, existing in the narrow and quasi linear domains (interstices and grooves), located inside and on the surface of a packed bundle. These domains disappear when the bundle is expanded, a disadvantage compensated by the increase of the specific surface.

The isosteric heat of the nanotube adsorbents are plotted in Figure 5. For the models where the internal and/or external surface of the nanotubes is accessible, the q_i values are similar to those of slit pore models. By contrast, the q_i values of the close-packed bundle of closed nanotubes differ because in this case the adsorption takes place at a large extent in narrow linear interstitial domains. As for the activated carbon models, the low pressure estimate of q_i is in a agreement with the exact formula below 5.0 MPa.

A quantitative comparison with previous simulations is made difficult by the fact that the V_f value of the studied models generally is not known. Therefore, the reported values of wt $\%_t$ include nonestimable compression effects. For instance, at 10.0 MPa and 298 K, in arrays of opened (9,9) (D_n = 1.22 nm) and (18,18) (D_n = 2.44 nm) SW nanotubes, Wang and Johnson[6] give wt $\%_t$ = 0.4 and 0.9. At 10.0 MPa and 293 K, Guay et al.[14] give for an array of opened (20,0) SW nanotubes with d = 0.4 and 0.6 nm: wt $\%_t$ = 0.7 and 1.2, respectively. Rzepka et al.[4] use a simplified nanotube model, with D_n = 1.0 nm, they find wt $\%_t$ = 0.6 at 10.0 MPa and 300 K. At 3.0 MP and 298 K, Gigras et al.,[17] in a square array of (9,9) SW nanotubes with d = 0.6 nm, compute wt $\%_t$ = 0.41. Clearly, the results are coherent with an adsorption capacity of the nanotube adsorbents such as wt $\%_t$, and so wt $\%_e$, are <1 at room temperature and pressures smaller than 10.0 MPa. But the model diversity and the only wt $\%_t$ values preclude a more precise estimate.

At 298 K, Smith et al.[13] determine the excess adsorption of close-packed bundles containing opened nanotubes of different diameters (average diameter $\sim$ 1.3 nm) by using an estimate of V_f, different of that used in this work. They obtain close values of wt $\%_e$ for all the considered bundles and, for instance with $d \sim 0.4$ nm, find at 1.0 MPa: wt $\%_e \sim 0.07$ and 4.8 MPa: wt $\%_e \sim 0.35$. Increasing by 30% the solid-hydrogen potential and for expanded bundles with $d \sim 0.64$ nm, they find at 1.0 MPa: wt $\%_e \sim 0.15$ and 4.8 MPa: wt $\%_e \sim 0.9$. At 293 K, we obtain for the close-packed bundle (d = 0.34 nm) of opened (17,0) nanotubes, at 1.0 MPa: wt $\%_e$ = 0.07, at 5.0 MPa: wt $\%_e$ = 0.27 and 10.0 MPa: wt $\%_e$ = 0.43, and for the expanded bundle (d = 0.6 nm) of opened (17,0) nanotubes, at 1.0 MPa: wt $\%_e$ = 0.11, at 5.0 MPa: wt $\%_e$ = 0.43 and 10.0 MPa: wt $\%_e$ = 0.70.

GNF models

As discussed earlier, the adsorbing surfaces of the nonexpanded GNF models are formed by functional groups CH or CH_3. It is possible to consider other chemical groups and, also, surfaces that are not uniformly functionalized by the

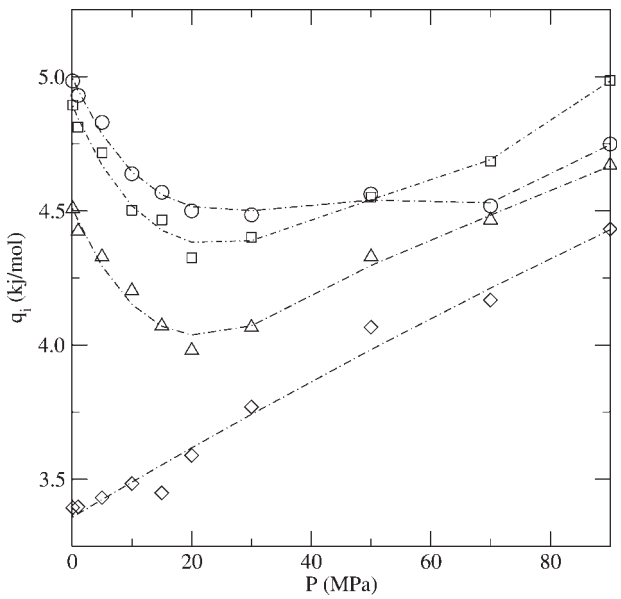

Figure 5. Isosteric heats q_i for bundles of 30 SW nanotubes of diameter D_n = 1.33 nm estimated from Eq. 3.

Close-packed bundle (d = 0.34 nm) of closed nanotubes: diamond and open nanotubes: square. Expanded bundle (d = 0.60 nm) of closed nanotubes: triangle up and open nanotubes: circle. Dashed-dotted lines: guide to the eyes.

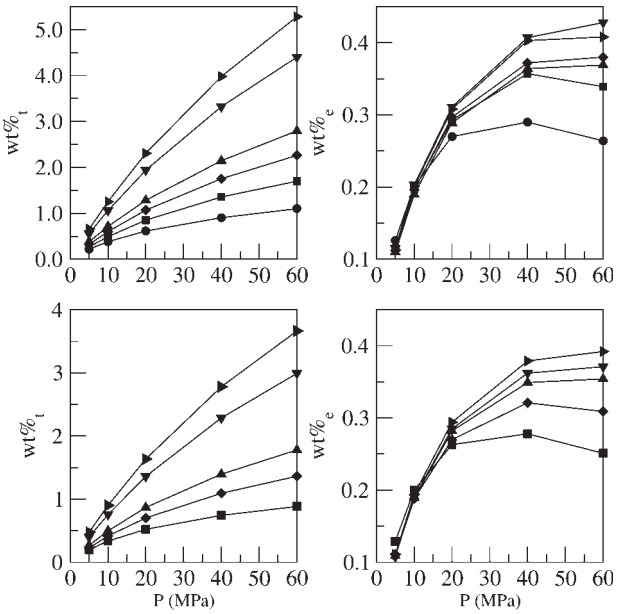

Figure 6. At T = 293 K, isotherms of the total (wt $\%_t$) and excess (wt $\%_e$) adsorption for the GNF1 models with surfaces functionalized by groups CH (top row) and CH_3 (bottom row) for different slit widths.

0.7 nm (circle), 1.0 nm (square), 1.3 nm (diamond), 1.6 nm (triangle up), 2.5 nm (triangle down), and 3.nm (triangle left).

same groups. But, CH and CH_3 have been chosen, because they have van der Waals interactions, which are representative of those of chemical groups (CO, O, OH,...) possibly bonded to the terminal carbon atoms of graphene sheets. Among these chemical groups, CH and CH_3 belong, respectively, to those with a weak or large van der Waals interaction. It was supposed that the excluded volume effects between CH_3 or CH groups, bonded to same or neighboring graphite planes, do not preclude a complete and uniform functionalization of the pore walls.

The total and excess adsorption isotherms of the GNF1 models are displayed in Figure 6 for the pore widths 0.7, 1.0, 1.3, 1.6, 2.5, and 3.0 nm. They correspond to adsorption capacities similar to those of the AC3 model, which has a quasi identical specific surface ~900 m^2/g. Similarly, to the activated carbon models at a given pressure, wt $\%_t$ increases almost proportionally to the pore width, but this increase is also due to the compression effects as it is seen from the plots of wt $\%_e$ in Figure 6. It seems unexpected that the wt $\%_e$ values of GNF1-CH are slightly larger than those of GNF1-CH_3 because the van der Waals interaction of CH_3 is stronger than that of CH. This fact mainly results from the increase of the adsorbent mass because of the addition of the CH_3 groups.

We present in Figure 7 the adsorption data of GNF2 models with an herringbone structure. In these models, the graphite planes in the stacks forming the pore walls are tilted by 30° with respect to the fiber axis and functionalized at their ends by CH groups. When the plane spacing d_p is equal to 0.34 nm, the total and excess adsorptions are slightly larger than those of the GNF1-CH model with the same slit width. This increase (~15–20%) results partly from the fact that the compression contribution is reduced because the free volume of the herringbone GNF2, for an identical slit width, is smaller than that of the GNF1 model.

When the GNF2 model is expanded by increasing d_p, the excess adsorption increases; in particular, for d_p equal to 0.9 nm, wt $\%_e$ becomes of the order of 2% for pressures larger than 40.0 MPa. These favorable results come from the open structure of the adsorbents, which allow to add to the adsorption on the terminal CH groups; the adsorption on the surfaces of the graphite planes estimated from the AC1 model results to wt $\%_e$ ~1%. The fact that the adsorption because of the CH groups and the graphite plane surfaces contribute at the same level is due to the small transverse size of the graphite plane (D = 1 nm) in the GNF2 models. For much larger values of D, the adsorption of the expanded GNF would be similar to that of the AC1 model, the contribution of the CH groups becoming marginal.

The isosteric heats of adsorption for GNF models are presented in Figure 8. The q_i values of the GNF1 models increase almost monotonically with the pressure. They show that q_i decreases with the slit width, as it is found also for the activated carbon models, and reaches an asymptotic value for d_s of the order of 2.5–3.0 nm. The plots displayed in Figure 8 show also that q_i for the GNF2 models decreases when the slit width increases and has a similar value to that of GNF1 model for identical width. The variation of q_i for a fixed slit width and given pressure as a function of d_p is nonmonotonic, in particular, at pressures below 30.0 MPa, but it

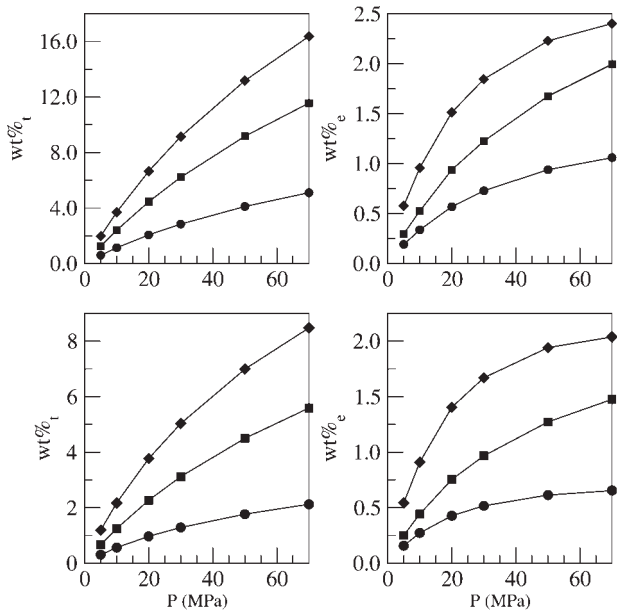

Figure 7. At T = 293 K, isotherms of the total (wt $\%_t$) and excess (wt $\%_e$) adsorption for the herringbone GNF2 models with surface functional groups CH and different slit widths d_s = 2.5 nm.

Top row and d_s = 1.0 nm: bottom row. Graphite plane spacing: d_p = 0.34 nm (filled circle), d_p = 0.68 nm (filled square), and d_p = 0.90 nm (filled diamond).

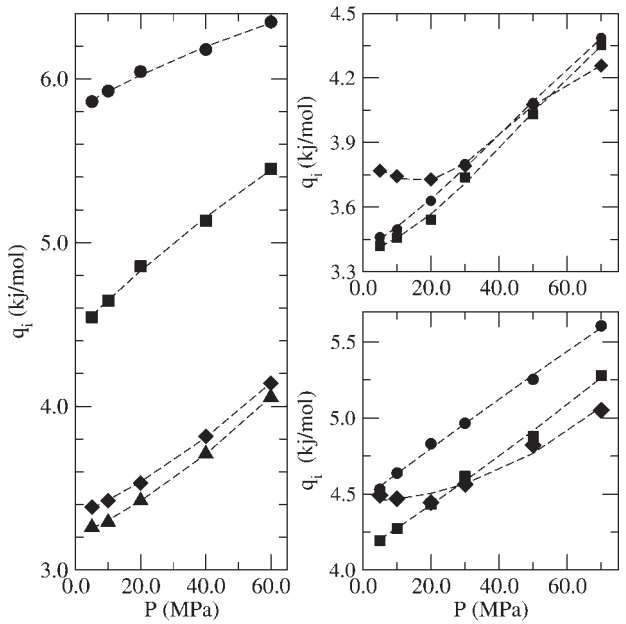

Figure 8. Left column: isosteric heats from Eq. 3 for the GNF1 models functionalized by groups CH.

Slit widths d_s = 0.7 nm: filled circle, d_s = 1.0 nm: filled square, d_s = 2.5 nm: filled diamond, and d_s = 3.0 nm: filled triangle up. Right column: isosteric heats from Eq. 3 for the herringbone GNF2 models functionalized by groups CH: slit widths d_s = 2.5 nm (top) and d_s = 1.0 nm (bottom). Graphite plane spacing d_p = 0.34 nm: filled circle, d_p = 0.68 nm: filled square, and d_p = 0.90 nm: filled diamond.

is important to remark that this evolution results from a complex process combining adsorption on a heterogeneous surface in different conditions of confinement between the stacks or the graphite planes.

The complexity of adsorption process in the expanded GNF is illustrated by the density profiles drawn in Figure 9. For d_p = 0.34 nm, no H_2 molecule can go inside the graphite plane stack, and the layers of adsorbed molecules are located on the stack surface. For d_p = 0.68 nm, H_2 molecules get in the space between the graphite planes, but, because of the excluded volume effects associated to the CH groups, the molecules are mainly adsorbed at the mid distance of the graphite plane ends. When d_p = 0.90 nm, the adsorption inside the interplane space increases and the local density is larger than the bulk density, although the CH group excluded volume effects stay yet visible.

Discussions and Conclusions

Simulations of H_2 adsorption have been realized for pore models of carbonaceous porous adsorbents (AC1, AC2, AC3, GNF1, and nonexpanded GNF2 models) and adsorbent models of SW nanotubes. They suppose that H_2 adsorption is a physisorption only because of van der Waals H_2-adsorbent interaction, although more complex chemical processes could possibly contributed.[46] A significant and unbiased comparison between the adsorption capacities can be performed, because each model is characterized in the same way. In particular, the specific surfaces have been estimated from the geometric sizes and atomic structures of the pore walls and the free volumes determine by simulations reproducing the experimental Helium displacement method.

From the simulations results, it appears that the slit pore models have an excess adsorption wt $\%_e$ which, at room temperature, stays smaller than 0.2–0.4 for pressures below 10.0 MPa. wt $\%_e$ increases toward a maximal values $\sim$1.0 for pressures larger than 40.0 MPa when the model has a specific surface equal to $\sim$2600 m^2/g. The agreement with experimental result is good for the activated carbon models where the comparison seems the most significant, because the experimental samples are well characterized and present a weak amount of impurities.[43,44,47–49]

For the nanotube adsorbent models, the experiment-simulation comparison is ambiguous. The nanotube samples often contain a large amount of impurities and the proportion of opened and closed nanotubes generally is not known.[43,44,50,51] It is important to stress that a comparison, realized with experimental or simulation data on the unique basis of the total adsorptions, can be misleading if the contribution of compression effects cannot be estimated. When this latter contribution is known, the excess adsorptions wt $\%_e$ computed by simulations or experimentally measured have the same order of magnitude and are smaller than 1.0%.

The GNF models have been studied to determine the adsorption capacities of GNF formed by stacks of graphite planes in the specific case where the adsorbing surface is constituted by functionalized carbon atoms. The results

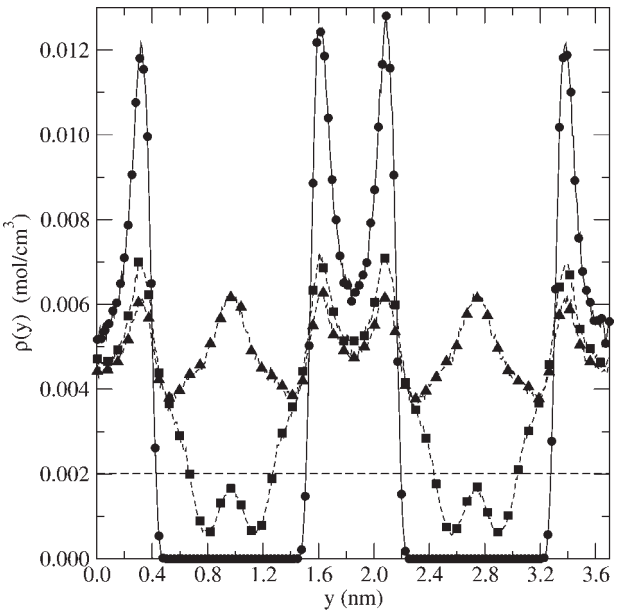

Figure 9. At T = 293 K, density profiles of H_2 adsorbed molecules for the GNF2 model with different spacings d_p between the graphite planes of the stacks for a pressure equal to 5.0 MPa.

The profiles $\rho(y)$ are computed in the direction y, perpendicular to the slit pores (width d_s = 1.0 nm). Solid line and filled circle d_p = 0.34 nm, dashed line and filled square d_p = 0.68 nm, and dashed line and filled triangle up d_p = 0.90 nm. Horizontal dashed line: bulk density.

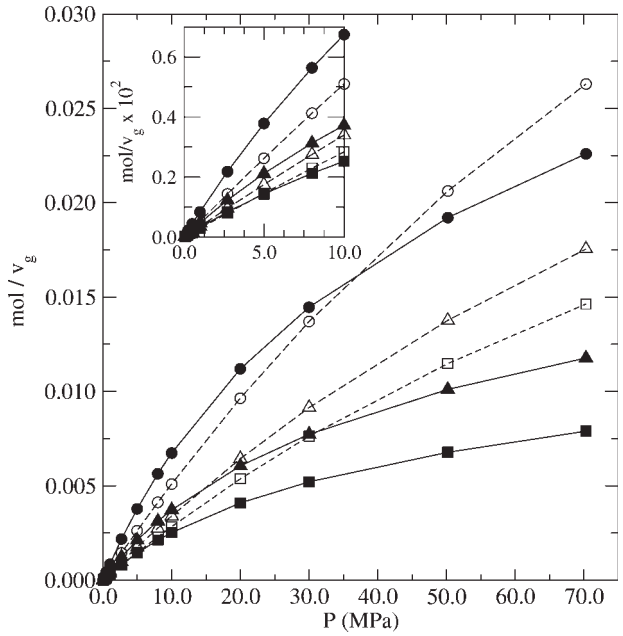

Figure 10. At T = 293 K, total amount of H_2 (mol) vs. pressure contained in a volume v_g exactly suitable for 1 g of AC1 (circle) (v_g = 1.314 cm^3, AC2 (triangle up) (v_g = 0.877 cm^3), or AC3 (square) (v_g = 0.732 cm^3) adsorbent with a slit width of 1.0 nm.

Dashed lines and open symbols: empty volume. Continuous lines and filled symbols: volume filled with the adsorbent. Inset: close view of the low pressure domain.

obtained for the nonexpanded GNF models give wt $\%_e$ values similar to those of the AC3 model. Although the interaction between H_2 and adsorbing site of the functionalized GNF is larger than in the activated carbons, the adsorption capacity of the GNF models stays close to that of the AC models mainly because of a low density of adsorbing sites on the GNF surfaces. For the expanded GNF models where the adsorption on graphite basal planes and CH sites is combined, it is possible to reach, at pressures above 40.0 MPa, a wt $\%_e$ value equal to $\sim$2.0.

The isosteric heats of the models vary between 3.5 and 6.5 kJ/mol. At low pressures, q_i values equal to $\sim$5.0 kJ/mol are characteristic of adsorption processes in narrow pores (size $<$1.0 nm).

With respect to the storage capacity of the carbonaceous adsorbents, Figure 10 shows, vs. pressure, the H_2 amounts stored in a given volume v_g empty or filled by the AC1, AC2, and AC3 adsorbents with a slit width equal to 1.0 nm. The amount of H_2 stored in v_g filled by the adsorbents exceeds that stored by compression in the empty volume below 35.0, 15.0, and 5.0 MPa for the AC1, AC2, and AC3 models, respectively. The amount in excess is marginal for the AC3 model. But it is of the order of $\sim$20% between 10.0 and 20.0 MPa for the AC1 model, possibly sufficient so that an activated carbon with an adsorption capacity near that of this model can be used at least in a static storage. It is worth to notice that, obviously, the adsorption capacity of nanoporous carbon materials is very insufficient to allow that these materials can be used for the storage H_2 in a car tank. This conclusion, obtained at room temperature, stays yet valid at temperature as lower as 77 K, as it is demonstrated in particular by GCMC simulations.[11,52]

In summary, our simulations show that the main classes of porous carbonaceous materials present similar adsorption capacities. The quantitative variations of these capacities induced by the differences of pore types are important but they stay too small to achieve an efficient storage of H_2 at room temperature.

Acknowledgments

This work, in particular the simulation of hydrogen adsorption in graphite nanofibers, was realized in the scope of Marie Curie Research Training Network HyTRAIN European Project (Reference Number: 512443).

Literature Cited

1. Yang RT. *Gas Separation by Adsorption Processes*. London: Imperial College Press, 1997.
2. Malbrunot P, Vidal D, Vermesse J, Chahine R, Bose TK. Adsorption measurements of argon, neon, krypton, nitrogen, and methane on activated carbon up to 650 MPa. *Langmuir*. 1992;8:577–580.
3. Lamari Darkrim F, Levesque D. Monte Carlo simulations of hydrogen adsorption in single-walled carbon nanotubes. *J Chem Phys*. 1998;109:4981–4984.
4. Rzepka M, Lamp P, de la Casa-Lillo MA. Physisorption of hydrogen on microporous carbon and carbon nanotubes. *J Phys Chem B*. 1998;102:10894–10898.
5. Lamari Darkrim F, Vermesse J, Malbrunot P, Levesque D. Monte Carlo simulations of nitrogen and hydrogen physisorption at high pressures and room temperature. Comparison with experiments. *J Chem Phys*. 1999;110:4020–4027.
6. Wang Q, Johnson JK. Molecular simulation of hydrogen adsorption in single-walled carbon nanotubes and idealized carbon slit pores. *J Chem Phys*. 1999;110:577–586.
7. Wang Q, Johnson JK. Computer simulations of hydrogen adsorption on graphite nanofibers. *J Phys Chem B*. 1999;103:277–281.
8. Darkrim F, Aoufi A, Levesque D. Quantum contribution to gas adsorption in carbon nanotubes. *Mol Simul*. 2000;24:51–61.
9. Darkrim F, Levesque D. High adsorptive property of opened carbon nanotubes at 77 K. *J Phys Chem B*. 2000;104:6773–6776.
10. Cracknell RF. Molecular simulation of hydrogen adsorption in graphitic nanofibres. *Phys Chem Chem Phys*. 2001;3:2091–2097.
11. Levesque D, Gicquel A, Lamari Darkrim F, Beyaz Kayiran S. Monte Carlo simulations of hydrogen storage in carbon nanotubes. *J Phys Condens Matter*. 2002;14:9285–9294.
12. Simonyam VV, Johnson JK. Hydrogen storage in carbon nanotubes and graphitic nanofibers. *J Alloys Compd*. 2002;330–332:659–665.
13. Smith MR, Bittner EW, Shi W, Johnson JK, Bockrath BC. Chemical activation of single-walled carbon nanotubes for hydrogen adsorption. *J Phys Chem B*. 2003;107:3752–3760.
14. Guay P, Stansfield BL, Rochefort A. On the control of carbon nanostructures for hydrogen storage applications. *Carbon*. 2004;42:2187–2193.
15. Shao X, Wang W, Xue R, Shen Z. Adsorption of methane and hydrogen on mesocarbon microbeads by experiment and molecular simulation. *J Phys Chem B*. 2004;108:2970–2978.
16. Mpourmpakis G, Froudakis GE, Lithoxoos GE, Samos J. Effect of curvature and chirality for hydrogen storage in single-walled carbon nanotubes: a combined ab initio and Monte Carlo investigation. *J Chem Phys*. 2007;126:144704.
17. Gigras A, Bhatia SK, Kumar AVA, Myers AL. Feasibility of tailoring for high isosteric heat to improve effectiveness of hydrogen storage in carbons. *Carbon*. 2007;45:1043–1050.
18. Silvera IF, Goldman VV. The isotropic intermolecular potential for H_2 and D_2 in the solid and gas phases. *J Chem Phys*. 1978;69:4209–4213.

19. Steele WA. *The Interaction of Gases with Solid Surfaces*. New York: Pergamon Press, 1974.
20. Crowell AD, Brown JS. Laterally averaged interaction potentials for $^1H_2$ and $^2H_2$ on the (0001) graphite surface. *Surf Sci*. 1982;123:296–304.
21. Nicholson D, Parsonage NG. *Computer Simulation and the Statistical Mechanics of Adsorption*. London: Academic Press, 1982.
22. Frenkel D, Smit B. *Understanding Molecular Simulation*. London: Academic Press, 2002.
23. Patrick JW, editor. *Porosity in Carbons*. London: Edward Arnold, 1995.
24. Stoeckli F, Centeno TA. On the determination of surface areas in activated carbons. *Carbon*. 2005;43:1184–1190.
25. Do DD, Do HD. GCMC-surface area of carbonaceous materials with N_2 and Ar adsorption as an alternative to the classical BET method. *Carbon*. 2005;43:2112–2121.
26. Dresselhaus MS, Dresselhaus G, Eklund PC. *The Science of Fullerenes and Carbon Nanotubes*. New York: Academic Press, 1996.
27. Calbi MM, Toigo F, Cole MW. Dilation-induced phases of gases absorbed within a bundle of carbon nanotubes. *Phys Rev Lett*. 2001;86:5062–5065.
28. Hwang JY, Lee SH, Sim KS, Kim JW. Synthesis and hydrogen storage of carbon nanofibers. *Synth Met*. 2002;126:81–85.
29. Chen X, Xu ZH, Li X, Shaibat MA, Ishii Y, Ruoff RS. Structural and mechanical characterization of platelet graphite nanofibers. *Carbon*. 2007;45:416–423.
30. Zhu YA, Sui ZhJ, Zhao TJ, Dai YCh, Cheng ZhM, Yuan WK. Modeling of fishbone-type carbon nanofibers: a theoretical study. *Carbon*. 2005;43:1694–1699.
31. Wilson AD, Nakanishi H, Kasai H, Sugimoto T, Kondo T. H_2 dissociative adsorption at the zigzag edges of graphite. *e-J Surf Sci Nanotech*. 2004;2:77–80.
32. Dresselhaus MS, Dresselhaus G. Intercalation compounds of graphite. *Adv Phys*. 2002;51:1–186.
33. Lueking AD, Pan L, Narayanan DL, Clifford CEB. Effect of expanded graphite lattice in exfoliated graphite nanofibers on hydrogen storage. *J Phys Chem B*. 2005;109:12710–12717.
34. Malbrunot P, Vidal D, Vermesse J, Chahine R, Bose TK. Adsorbent helium density measurement and its effect on adsorption isotherms at high pressure. *Langmuir*. 1997;13:539–544.
35. Kaneko K, Cracknell RF, Nicholson D. Nitrogen adsorption on slit pores at ambient temperature: comparison of simulation and experiment. *Langmuir*. 1994;10:4606–4609.
36. Marx D, Nielaba P. Path-integral Monte Carlo techniques for rotational motion in two dimensions: quenched, annealed and no-spin quantum-statistical averages. *Phys Rev*. 1002;45:8968–8971.
37. Georgiev PA, Ross DK, Albers P, Ramirez-Cuesta AJ. The rotational and translational dynamics of molecular hydrogen physisorbed in activated carbon: a direct probe of microporosity and hydrogen storage performance. *Carbon*. 2006;44:2724–2738.
38. Martin MG, Siepmann JI. Transferable potentials for phase equilibria. I. United-atom description of *n*-alkanes. *J Phys Chem B*. 1998;102:2569–2577.
39. Bourasseau E, Haboudou M, Boutin A, Fuchs A, Ungerer P. New optimization method for intermolecular potentials: optimization of a new anisotropic united atoms potential for olefins: prediction of equilibrium properties. *J Chem Phys*. 2003;118:3020–3034.
40. Vuong T, Monson PA. Monte Carlo simulation studies of heats of adsorption in heterogeneous solids. *Langmuir*. 1996;12:5425–5432.
41. Lamari M, Aoufi A, Malbrunot P. Thermal effects in dynamic storage of hydrogen by adsorption. *AIChE J*. 2000;46:632–646.
42. Bhatia SK, Myers AL. Optimum conditions for adsorptive storage. *Langmuir*. 2006;22:1688–1700.
43. Beyaz Kayiran S, Lamari Darkrim F, Levesque D. Adsorption properties and structural characterization of activated carbons and nanocarbons. *J Phys Chem B*. 2004;108:15211–15215
44. de la Casa-Lillo MA, Lamari-Darkrim F, Cazorla-Amorós D, Linares-Solano A. Hydrogen storage in activated carbons and activated carbon fibers. *J Phys Chem B*. 2002;106:10930–10934.
45. Farhat S, Weinberger B, Lamari Darkrim F, Izouyar T, Noe L, Monthioux M. Performance of carbon arc-discharge nanotubes to hydrogen energy. *J Nanosci Nanotechnol*. 2007;7:1–6.
46. Meregalli V, Parrinello M. Review of theoretical calculations of hydrogen storage in carbon-based materials. *Appl Phys A*. 2001;72:143–146.
47. Ahn CC, Ye Y, Ratnakumar BV, Witham C, Bowman RC Jr, Fuitz B. Hydrogen desorption and adsorption measurements on graphite nanofibers. *Appl Phys Lett*. 1998;73:3378–3380.
48. Johansson E, Hjörvarsson B, Ekström T, Jacob M. Hydrogen in carbon nanostructures. *J Alloys Compd*. 2002;330–332:670–675.
49. Züttel A, Nüzenadel Ch, Sudan P, Mauron Ph, Emmenegger Ch, Remtsch S, Schlapbach L, Weidenkaff A, Kiyobayashi T. Hydrogen sorption by carbon nanotubes and other carbon nanostructures. *J Alloys Compd*. 2002;330–332:676–682.
50. Murata M, Kaneko K, Kanoh H, Kasuya D, Takahashi K, Kokai F. Adsorption mechanism of supercritical hydrogen in internal and interstitial nanospaces of single-wall carbon nanohorn assembly. *J Phys Chem B*. 2002;106:11132–11138.
51. Anson A, Callejas MA, Benito AM, Maser WK, Izquierdo MT, Rubio B, Jagiello J, Thommes M, Parra JB, Martinez MT. Hydrogen adsorption studies on single wall carbon nanotubes. *Carbon*. 2004;42:1243–1248.
52. Kowalczyk P, Holyst R, Terrones M, Terrones H. Hydrogen storage in nanoporous carbon materials: myth and facts. *Phys Chem Chem Phys*. 2007;9:1786–1792.

Manuscript received July 7, 2007, revision received Jun. 12, 2008, and final revision received Aug. 21, 2008.